Applied Catalysis B: Environmental 340 (2024) 123213

Contents lists available at ScienceDirect

Applied Catalysis B: Environmental

journal homepage: www.elsevier.com/locate/apcatb

Heterogeneous catalytic reactions of *in-situ* generated bromide ions *via* hydrodehalogenation of tetrabromobisphenol A in advanced oxidation processes over palladium nanoparticles

Yang Wu [a], Lang Chen [a], Pengliang Sun [a], Qingran Zhang [a,c], Yinguang Chen [a,c], Xiong Zheng [a,b,c,*]

[a] State Key Laboratory Of Pollution Control And Resource Reuse, School of Environmental Science and Engineering, Tongji University, Shanghai 200092, China
[b] Key Laboratory of Yangtze River Water Environment, School of Environmental Science and Engineering, Tongji University, Shanghai 200092, China
[c] Shanghai Institute of Pollution Control and Ecological Security, Shanghai 200092, China

ARTICLE INFO

Keywords:
Advanced oxidation process
Liquid-phase catalytic hydrodehalogenation
Bromide ions
Palladium nanoparticles
Singlet oxygen ($^1O_2$)

ABSTRACT

Herein, we report a novel and efficient approach for degrading tetrabromobisphenol A (TBBPA) *via* catalytic hydrodehalogenation (HDH) and advanced oxidation processes (AOP). Using heterogeneous catalytic HDH of TBBPA over palladium nanoparticles (Pd NPs) achieves the *in-situ* generation of bromide ions (Br^-), which effectively accelerate and reinforce the degradation of debromination intermediates during peroxymonosulfate-based AOP. The conversion of TBBPA to bisphenol A (BPA) by the HDH process reaches up to 99.9% debromination efficiency in 1 h under near-neutral condition, along with the removal of 99.4% BPA in 15 min during the AOP. Further studies show that free bromine and $^1O_2$ produced by *in-situ* generated Br^- reacting with peroxymonosulfate are the most effective reactive species for promoting the BPA degradation. Sustainability footprint analysis reveals considerable stability and high sustainable footprint of the integrated process during long-term operation. This work provides a promising strategy to elimination of bromine organic pollutants in water treatment.

1. Introduction

Due to their exceptional flame-retardant properties, brominated flame retardants (BFRs) find extensive use in a variety of consumer products, including electronics, construction materials, and plastics. Consequently, they account for more than one-fifth of the total production of flame retardants [1]. Among the BFRs, tetrabromobisphenol A (TBBPA) is a widely utilized compound worldwide, experiencing an annual market demand growth rate of 3.4% [2]. Throughout its lifecycle, from production to utilization and disposal, TBBPA inevitably enters aquatic environments, leading to its ubiquitous presence [3]. For example, in river sediments near electronics factories, TBBPA concentrations have been reported to range from 84.0 to 646.1 ng/g dry weight (dw) [4]. Moreover, TBBPA exhibits a propensity for bioaccumulation, becoming enriched in living organisms through the food chain. Concentrations of TBBPA in human breast milk and umbilical cord serum have been measured at 37.3 and 649.45 ng/g, respectively [5]. Nevertheless, TBBPA is recognized as an endocrine disruptor and immunotoxicant, with the potential to induce cytotoxic, neurotoxic, and immunotoxic effects, thereby posing a threat to human health [6,7]. Consequently, it is of great importance and value to develop a safe and efficient method for the removal of TBBPA from aquatic environments.

Advanced oxidation process (AOP) is a highly effective technique for the removal of TBBPA due to its robust oxidation capability and potential for mineralization using reactive oxygen species (ROS, *e.g.*,·OH, and $SO_4{\cdot}^-$, and $^1O_2$) [8]. However, incomplete debromination during AOP can result in the generation of more toxic brominated by-products [9]. Liquid-phase catalytic hydrodehalogenation (HDH) provides a promising approach to address the debromination deficiency of BFRs under mild and environmentally friendly reaction conditions [10]. Nevertheless, the successful implementation of this integrated strategy faces a challenge in finding an efficient catalyst that can synergistically enhance *in-situ* HDH and AOP for BFRs removal. Noble metals, particularly Pd, have demonstrated exceptional activity in breaking

* Corresponding author at: State key laboratory of pollution control and Resource reuse, School of Environmental Science and Engineering, Tongji University, Shanghai 200092, China.
E-mail address: xiongzheng@tongji.edu.cn (X. Zheng).

https://doi.org/10.1016/j.apcatb.2023.123213
Received 14 June 2023; Received in revised form 20 August 2023; Accepted 22 August 2023
Available online 23 August 2023

carbon-halogen bonds, attributed to their ability to selectively absorb and store H* [11]. These catalysts also hold potential for AOP, with Pd nanoparticles (Pd NPs) demonstrating higher activity compared to transition metal nanocatalysts like Mn and Co [12]. However, traditional HDH methods suffer from poor mass transfer, necessitating continuous flushing of H_2 [11,13] resulting in low gas utilization efficiency (<5%) and potential safety risks. Additionally, the direct addition of catalysts can lead to agglomeration and losses with the effluent, thereby reducing catalytic efficiency [14]. Thus, the deposition of Pd NPs on non-porous hollow-fiber membranes presents a promising solution to overcome these limitations. This approach enables the spontaneous transfer of H_2 to Pd NPs under inherent pressure and facilitates the *in-situ* catalysis of both HDH and AOP, necessitating a comprehensive exploration of its potential benefits.

Moreover, the degradation of TBBPA during catalytic HDH predominantly involves a debromination process, converting TBBPA into bisphenol A (BPA) and bromide ions (Br^-) [13]. Previous work has shown that exogenous addition of Br^- has demonstrated reactivity towards phenolic structures during AOP when reacting with peroxymonosulfate (PMS) [15]. However, it remains uncertain whether *in-situ* generated Br^- through the catalytic HDH of TBBPA over Pd NPs can efficiently undergo oxidation by PMS, subsequently promoting BPA (as a typical phenolic structural pollutant) degradation. Furthermore, multiple reactive species (*e.g.*, Pd NPs, Br^-, and ROS) are likely involved in the AOP for the degradation of debromination intermediates. Understanding the formation and contribution of these reactive species in the overall degradation process is yet to be elucidated. Besides, assessing the sustainable footprint is essential to evaluate the operational performance and environmental sustainability of water treatment technologies [16]. Therefore, it is imperative to comprehensively compare the advantages and disadvantages of new and conventional methods in order to thoroughly investigate this innovative catalytic treatment.

The objective of this study was to investigate the enhanced degradation of TBBPA using *in-situ* generation of Br^- *via* heterogeneous catalytic HDH during the AOP over Pd NPs and elucidate the underlying mechanisms. Initially, the removal efficiencies of TBBPA and BPA were assessed individually during catalytic HDH and AOP over Pd NPs, respectively. Subsequently, the transformation of reactive species and their impacts on pollutant removal were comprehensively investigated. Furthermore, the removal performance of TBBPA was characterized during the integrated HDH-AOP over Pd NPs, and the degradation pathways and toxicities of intermediate products were predicted. Finally, the sustainable footprint of this novel catalytic treatment was assessed through an analysis of ranking efficiency products. This work presents a novel strategy for the elimination of BFRs and provides an in-depth understanding of the crucial role played by *in-situ* generated Br^- *via* heterogeneous catalytic HDH of TBBPA over Pd NPs during AOP for water treatment.

2. Materials and methods

2.1. Configuration of Pd NPs-supported membrane reactor

The reactor configuration is depicted in Fig. 1A (adapted from our previous publication [17]). The reactor consisted of two hollow glass tubes, each with a working volume of 40 mL, housing 60 identical hollow-fiber membranes. These non-porous polypropylene fibers, provided by Teijin (Japan), had an outer diameter of 200 μm and an inner diameter of 100 μm. High-purity H_2 gas (99.9%) was purged into both ends of the membranes and controlled by a pressure regulator. A circulating pump was employed to ensure solution circulation between the two tubes at a flow rate of 100 mL/min. The deposition of Pd NPs onto the membrane was accomplished using an *in-situ* H_2 reduction method. Initially, oxygen-free and fresh Na_2PdCl_4 (Sigma Aldrich, USA) with a purity of 99.9% was introduced to the reactor at a concentration of 0.1 mM, equivalent to 20 mg-Pd/m^2. Subsequently, H_2 gas was supplied at a pressure of 10 psig, and the circulating pump was activated. The Pd(II) ions were spontaneously reduced to Pd(0) NPs by H_2 and deposited onto the membrane surface. After 24 h of operation, the concentration of soluble Pd(II) was negligible, indicating complete

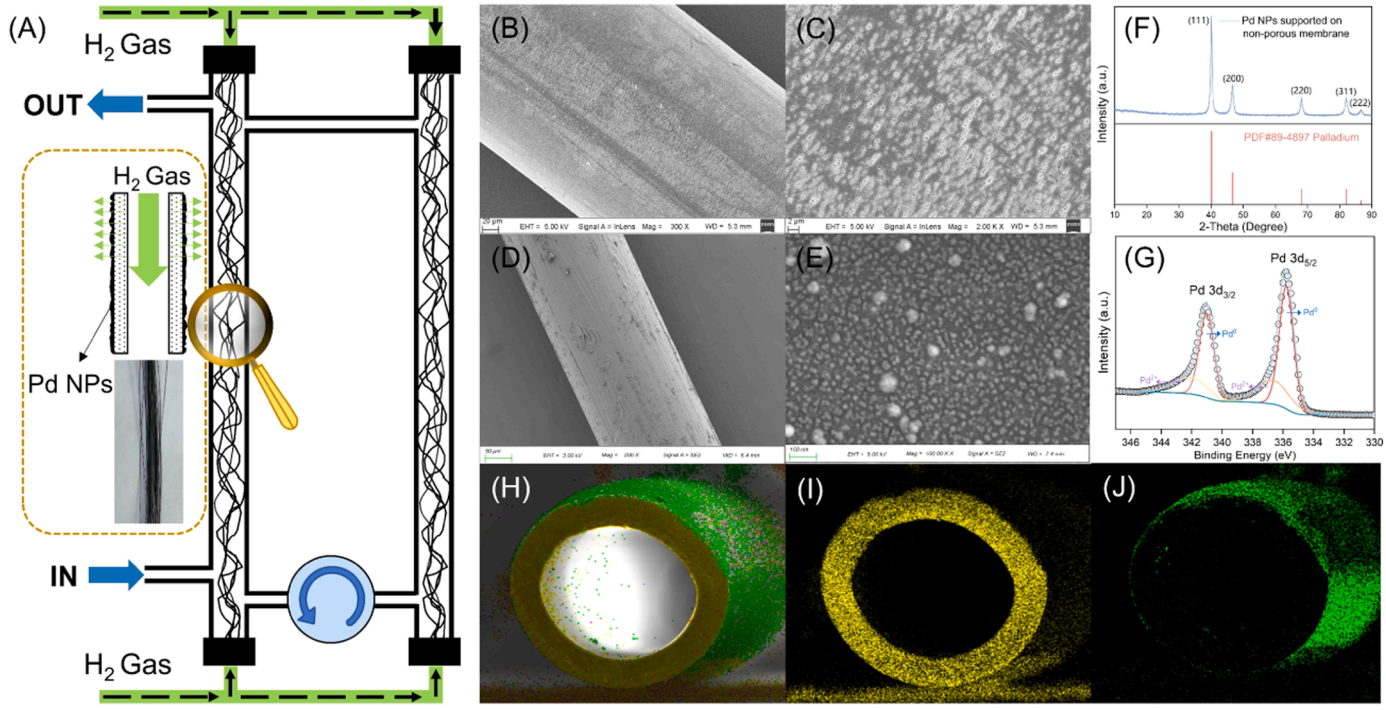

Fig. 1. The schematic diagram of the Pd NPs-supported membrane reactor (A), the SEM images of the raw non-porous membrane (B) and (C), the SEM image of the Pd NPs-supported membrane (D) and (E), the XRD analysis (F), the XPS analysis (G) and EDS-Mapping (yellow and green represented carbon and palladium, respectively) (H), (I) and (J) of Pd NPs supported on the surface of the membrane.

loading of Pd NPs onto the membrane. Finally, the reactor was subjected to two washes with ultrapure water to eliminate impurities before further experimentation.

2.2. Experiments for impacts of pH on the heterogeneous catalytic HDH of TBBPA over Pd NPs

To maintain an anaerobic environment, the reactor was purged with high-purity N_2 gas for 30 min prior to the experiments. A concentration of 25 mg/L of TBBPA (98% purity, Sigma Aldrich, USA) was introduced into the reactor, followed by the supply of H_2 gas at a pressure of 10 psig and the activation of the circulating pump. Since TBBPA is generally insoluble in acidic conditions [18], the initial pH value was adjusted to 7, 8, 9, and 10 using 0.1 mM H_2SO_4/NaOH to investigate the influences of pH values on the degradation of TBBPA during the heterogeneous catalytic HDH over Pd NPs. At regular intervals, 0.5 mL samples were extracted and immediately filtered through 0.22 μm filter membranes for subsequent determination of TBBPA, BPA, and Br^-.

2.3. Experiments for impacts of bromide ions on the AOP of BPA over Pd NPs

Since the primary products of TBBPA during heterogeneous catalytic HDH over Pd NPs are Br^- and BPA, 10 mg/L BPA (97% purity, Sigma Aldrich, USA) and 20.8 mg/L KBr (99% purity, Sigma Aldrich, USA) (equivalent to the concentration Br^- in TBBPA) were prepared in ultrapure water. The pH value was adjusted to 5, which corresponds to the final pH during catalytic HDH over Pd NPs for TBBPA degradation. The mixture was injected into the reactor, and then 1 mM PMS was added to initiate BPA degradation. At regular intervals, 0.5 mL of the filtered sample was collected and immediately mixed with 0.5 mL of methanol (MeOH) for further analysis. Furthermore, to ascertain the specific roles of Pd NPs and Br^- individually, separate AOP experiments for BPA removal were conducted with the sole presence of Pd NPs and Br^-, respectively. Moreover, to quantify the influence of reactive species on the AOP for BPA removal, MeOH (scavenger of·OH and $SO_4^{\cdot-}$ radical) [11], TBA (tert butyl alcohol, scavenger of·OH radical), L-histidine (scavenger of $^1O_2$), and ammonium (ammonium hydroxide, scavenger of free bromine ($HOBr/OBr^-$)) [15] were added to the mixture during the AOP.

2.4. Experiments for efficiency and degradation products of integrated HDH-AOP of TBBPA over Pd NPs

To investigate the removal efficiency of TBBPA during the integrated HDH-AOP over Pd NPs, the reactor was initially operated for 1 h to achieve heterogeneous catalytic HDH over Pd NPs supported on non-porous hollow-fiber membranes with the supply of 10 psig H_2 gas. Subsequently, 1 mM PMS was added to perform the subsequent AOP over Pd NPs for 1 h. At regular intervals, 0.5 mL samples were extracted and immediately mixed with 0.5 mL of MeOH to determine the concentrations of TBBPA and BPA. Additionally, to identify the intermediate degradation products during the AOP over Pd NPs supported on the non-porous membrane, a 5 mL sample was subjected to solid phase extractions (SPE). The concentrated sample was then analyzed using ultra-performance liquid chromatography quadrupole time-of-flight mass spectrometry (UPLC-Q-TOF MS) for further analysis.

2.5. Analytical methods

The Pd NPs-supported membrane was first dried in the vacuum dry oven, and then cut into 2 cm pieces using liquid nitrogen. The morphology and distribution of Pd NPs on the non-porous hollow-fiber membrane were examined using scanning electron microscopy (SEM, S-480, HITACHI, Japan) coupled with energy-dispersive X-ray micro-analysis (EDS). The crystallographic structure of the synthesized materials was determined using X-ray diffraction (XRD) with an X-ray diffractometer (D8 Advance X, Bruker, Germany). X-ray photoelectron spectroscopy (XPS) spectra were recorded using a spectrophotometer (5000 C ESCA, PHI, USA) to analyze the elemental compositions of Pd NPs. Moreover, to determine the stability of catalysts, an entire bundle of fiber membranes coated with Pd NPs was subjected to microwave-assisted total digestion [19], and the Pd concentrations of the digested solutions and the effluent were determined by ICP-MS (PerkinElmer NexION 300X, USA).

The concentrations of TBBPA and BPA were measured using high-performance liquid chromatography (HPLC, 1260, Agilent, USA) with a Zorbax liquid chromatography column (SBC18, 2.1 mm × 100 mm, 1.8 μm, Agilent, USA) and a UV detector (wavelength 280 nm). The mobile phases consisted of MeOH (A) and ultrapure water with 0.1% formic acid (B), and gradient elution was employed with a flow rate of 0.3 mL/min. The initial mobile phase composition was 40% A, which was increased linearly to 90% A within 4 min. After a 2-minute hold, the mobile phase was decreased to 40% A at 7 min. The concentration of Br- was determined by ion chromatography (ICS500, DNEX, USA) at a flow rate of 0.8 mL/min. The level of TBBPA mineralization was measured using a total organic carbon analyzer (TOC-L, SHIMADZU, Japan).

To identify degradation intermediates, solid-phase extraction (SPE) was performed using hydrophilic-lipophilic balance cartridges (200 mg/6 mL, OASIS, USA) for desalination. The column was first activated with 5 mL of MeOH and 5 mL of acidic ultrapure water (pH = 2). Then, 5 mL of the sample was passed through the column, followed by the addition of 10 mL of ultrapure water to remove impurities. The intermediate was eluted with 10 mL of MeOH, and the obtained sample was concentrated to 2 mL by purging with high-purity N_2. Subsequently, ultra-performance liquid chromatography quadrupole time-of-flight mass spectrometry (UPLC-Q-TOF MS, Impact II, Bruker Daltonics, USA) with an Acquity BEH C18 column (100 mm × 2.1 mm, 1.7 μm, Waters) was used for analysis. The mobile phases consisted of ultrapure water with 0.1% formic acid (A) and MeOH (B), and gradient elution was employed with a flow rate of 0.3 mL/min. The operation parameters were similar to those used for HPLC analysis of TBBPA and BPA. Mass analyses were conducted in negative mode using electrospray ionization (ESI) as the ionization source.

The formation of $^1O_2$ was measured by electron paramagnetic resonance (EPR) method. Briefly, 5 mg samples (Pd-membrane, KBr, and Pd-membrane+KBr) were firstly separately mixed with 1 mL of ultrapure water. Then, the pH of these solutions was then adjusted to 5. Subsequently, 100 mM 2,2,6,6-tetramethyl-4-piperidine (TEMP) was added to each solution, and the reaction was initiated by the introduction of 2 mM PMS. The EPR spectra of $^1O_2$ were recorded using an EPR spectrometer (Bruker ELEXSYS 580, Germany).

To comprehensively evaluate the performance and sustainability aspects of TBBPA removal techniques, it is necessary to consider multiple factors simultaneously. The analytical model used in this study is known as the Ranking Efficiency Product (REP), which is based on previous methodologies [16]. This approach is inherently stochastic and relies on rank product statistics. For each technology j, the model evaluates and ranks each of the n independent characteristics between a minimum rank, $r_{i\text{-}MIN}$, and a maximum rank, $r_{i\text{-}MAX}$. The overall REP of a technology j is then calculated using Eq. 1.

$$REP = \left[\prod_{i=1}^{n} \left(r_i / r_{i-MAX}\right)_j\right]^{1/n} \quad (1)$$

where r_i represents the individual ranking score for characteristic i of technology j. The REP, as defined above, ranges between ($r_{i\text{-}MIN}/r_{i\text{-}MAX}$) and 1, representing the performance of the technology j from worst to best, respectively.

2.6. Theoretical calculation

All calculations were performed using the Gaussian 16 software package. The B3LYP functional was employed to calculate Gibbs free energy changes. Geometry optimization and frequency calculations were carried out using the 6–311 G(d) basis set to determine the optimal geometries for each compound. Singlet point energy calculations were conducted using the larger def2-TZVP basis set (TZVP). To account for weak interactions, the DFT-D3 with BJ-damping (D3BJ) method was applied to improve calculation accuracy. In general, the calculation was fully optimized at the B3LYP-D3BJ/TZVP level of theory. The IEFPCM implicit solvation model was utilized to incorporate the solvation effect. The Gibbs free energy of each compound was obtained by combining the single point energy with the previously calculated free energy correction terms. The Gibbs free energy change for the binding process was determined by subtracting the Gibbs free energy of the product from that of the reactant.

To identify the active sites in TBBPA and BPA, the structure of the compound under investigation was fully optimized at the B3LYP-D3BJ/TZVP level of theory. The 6–311 G(d) basis set was used for geometry optimization and frequency calculations. The solvation effect of water was considered using the solvation model based on density (SMD). Vibrational frequencies of the optimized structure were calculated at the same level to ensure it corresponds to a local energy minimum on the potential energy surface. The verification of real vibrational frequencies was performed. The Fukui index of M was determined using the Multiwfn software at the same level. The molecular orbital levels of the studied compounds, including the highest occupied molecular orbital (HOMO) and the lowest unoccupied molecular orbital (LUMO), were investigated through theoretical calculations. The Visual Molecular Dynamics (VMD) program was employed to generate color-filled iso-surface graphs for visualizing the molecular electrostatic potential (MESP) and molecular orbitals.

2.7. Statistical analysis

All experiments and tests in this study were performed in triplicate. Analysis of variance was used to test the significance of the obtained results, and $p < 0.05$ was considered to be statistically significant.

3. Results and discussion

3.1. Morphology and structure of Pd NPs supported on non-porous hollow-fiber membrane

Fig. 1B-J present the solid-state properties of a non-porous hollow-fiber membrane with 20 mg/m^2 Pd-NPs supported on its surface. The raw non-porous membrane comprised multiple layers of polymeric organic fibers (Fig. 1B and C), facilitating gas diffusion. Following catalyst deposition, the membrane surface became rough and covered

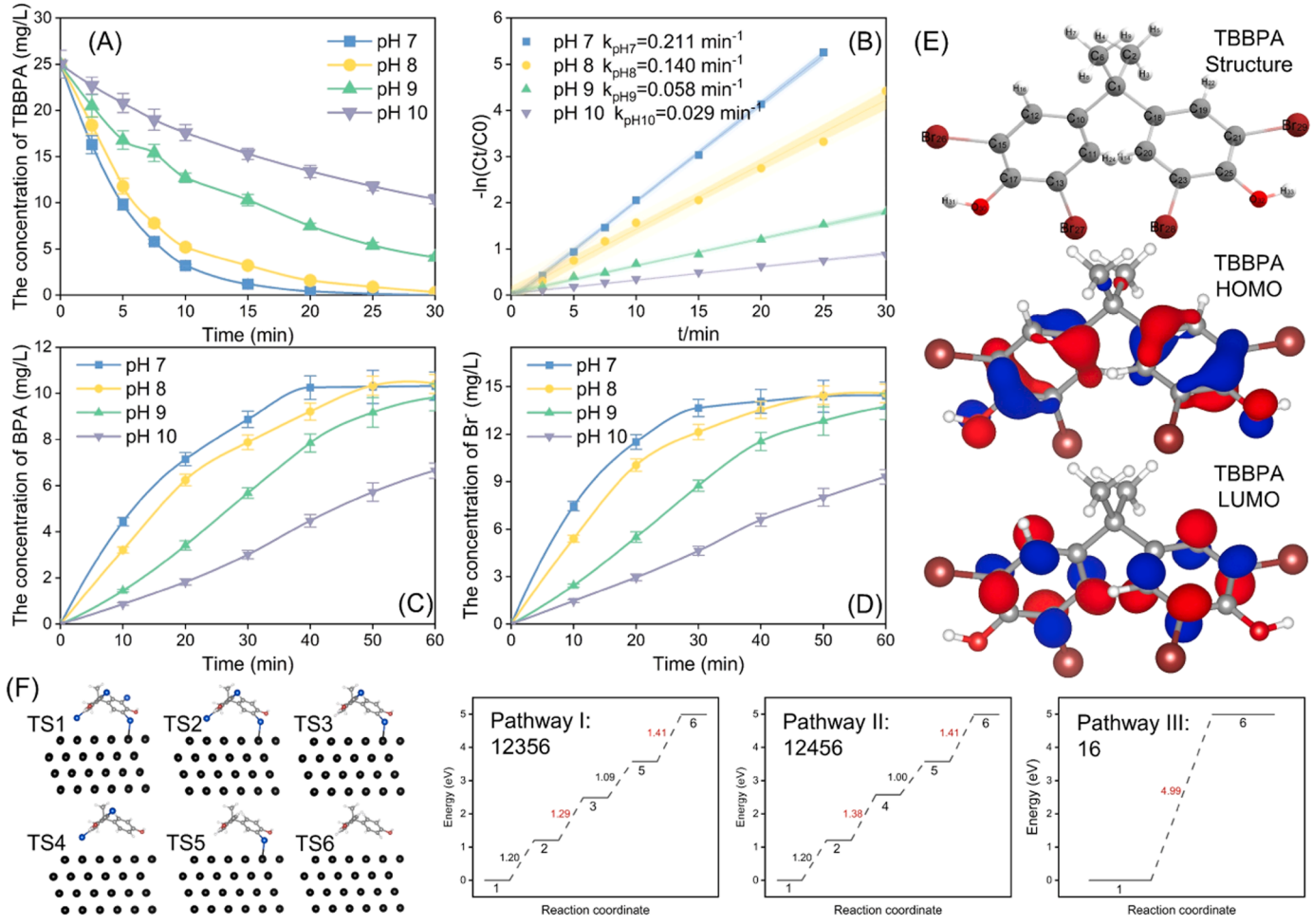

Fig. 2. The influence of initial pH value on TBBPA degradation during the heterogeneous catalytic HDH over Pd NPs (initial TBBPA 25 mg/L, Pd-loading 20 mg-Pd/m^2, gas pressure 10 psig): The variation of TBBPA (A), BPA (C) and Br$^-$ (D), the fitting curve applied by the Langmuir-Hinshelwood model (B), the chemical structure, the highest occupied molecular orbitals (HOMO), the lowest unoccupied molecular orbitals (LUMO) of TBBPA with the iso value of 0.04 (E), and the Gibbs free energy changes of TBBPA degradation during the heterogeneous catalytic HDH over Pd NPs (F).

with dispersed nanoparticles ranging from 10 to 30 nm (Fig. 2D and E). XRD analysis revealed five distinct diffraction peaks (2-Theta = 40.1, 46.6, 68.1, 82.1, and 86.7), corresponding to the characteristic peaks of pure Pd (PDF#89–4897) (Fig. 1F). Additionally, XPS analysis indicated that the two prominent peaks at 335.7 and 341.0 eV were associated with Pd(0), while the two negligible shoulders at 336.6 and 342.0 eV represented Pd(II) (Fig. 1G) [20], suggesting that Pd NPs predominantly existed in the form of Pd(0) on the membrane. Furthermore, EDS mapping analysis demonstrated dense and uniform distribution of the green-colored Pd on the membrane surface (Fig. 1H, I, and J), providing further evidence of the successful loading of Pd NPs onto the membrane. Overall, these results clearly illustrate the autocatalytic synthesis and spontaneous deposition of dispersed Pd NPs on the surface of the non-porous hollow-fiber membrane, highlighting their potential as efficient and *in-situ* catalysts for integrated HDH-AOP processes aimed at TBBPA removal from aquatic environments.

3.2. Effects of pH on the efficiency of liquid-phase catalytic HDH for TBBPA degradation over Pd NPs

The dissociation rate of H_2 *via* Pd NPs, which directly impacts the debromination efficiency during heterogeneous catalytic HDH, is closely related to pH values [11]. Therefore, the influence of initial pH value on TBBPA degradation over Pd NPs during catalytic HDH was investigated. Since TBBPA is nearly insoluble under acidic conditions, initial pH values of 7, 8, 9, and 10 were selected [18]. As shown in Fig. 2A, near-neutral conditions (pH = 7 and pH = 8) efficiently removed almost 99.9% of TBBPA within 30 min. As the initial pH increased, the degradation efficiency of TBBPA decreased accordingly. Additionally, fitting the Langmuir-Hinshelwood model demonstrated that TBBPA degradation during heterogeneous catalytic HDH over Pd NPs followed a pseudo-first-order kinetic model [13] (Fig. 2B). The rate constants were determined to be 0.211, 0.140, 0.058, and 0.029 min^{-1} when the initial pH values were 7, 8, 9, and 10, respectively, further indicating the effective removal of TBBPA under near-neutral conditions.

A previous study indicated that the heterogeneous HDH process for TBBPA removal involves both partial debromination (tri-BBPA, di-BBPA, and mono-BBPA) and complete debromination leading to the formation of BPA [21]. In this work, TBBPA was observed to undergo effective degradation within 30 min, while the maximum concentrations of BPA and Br^- were reached at 60 min. Furthermore, mass balance analysis demonstrated that the concentrations of BPA and Br^- at 60 min were approximately equal to the initial TBBPA content (Fig. 2C and D), indicating the achievement of complete debromination with BPA and Br^- as the final end products. Notably, the catalytic debromination activity of Pd NPs supported on the non-porous membrane exhibited a remarkable enhancement, being 2–3 orders of magnitude higher compared to other immobilized Pd-based materials [13,21–23]. This significant enhancement can be attributed to the presence of small and dispersed Pd NPs (Fig. 1E), which provide a larger specific surface area and a higher number of active sites. Additionally, the utilization of H_2 was highly efficient (>99.9%) with low H_2 consumption (approximately 5 mL H_2 in 60 min), surpassing the performance reported in previous works [13, 20–22].

The DFT analysis was conducted to identify the active sites in TBBPA. The Fukui index on the nucleophilic attack (f-) of four bromine atoms (26(Br), 29(Br), 27(Br), and 28(Br)) was found to be the highest (0.077, 0.077, 0.0576, and 0.0576) among all the atoms (Fig. 2E and Table S2), indicating their susceptibility to H* attack [24]. Hence, the debromination of TBBPA into BPA during HDH is very easy to occur driven by Pd NPs and H_2. Furthermore, to investigate whether the debromination process of TBBPA during catalytic HDH over Pd NPs was a step-by-step or a one-step reaction, the Gibbs free energy changes for different pathways were calculated (Fig. 2F). Although the total endothermic energy of all pathways was 4.99 eV, step-by-step reactions (Pathway I and II) were found to be more feasible as each step required less energy compared to the one-step reaction (Pathway III). These findings also explained the reason why the complete debromination time of TBBPA was later than the degradation time of TBBPA during HDH. In summary, the Pd NPs supported on the non-porous membrane demonstrated excellent catalytic activity for the HDH of TBBPA under near-neutral conditions, accompanied by efficient H_2 mass transfer.

3.3. In-situ generated bromide ions via HDH of TBBPA promoted BPA degradation in AOP over Pd NPs

Despite the effectiveness of catalytic HDH in addressing the debromination deficiency of TBBPA during the AOP, it still results in the formation of BPA as the final product due to its relatively weak ring-opening ability [21]. Therefore, BPA was selected as the model contaminant to investigate its further degradation during the AOP. As depicted in Fig. 3A, negligible degradation efficiency (3.4% in 60 min) was observed in the absence of chemical agents. However, in the presence of Pd NPs or Br^- individually, approximately 92.1% and 99.7% of BPA could be degraded in 60 min and 30 min, respectively. Moreover, when Pd NPs and Br- coexisted, the rate of BPA removal was significantly enhanced, reaching 99.4% within just 15 min. The mineralization rate of BPA could also reach ~60%. The degradation results were fitted to the Langmuir-Hinshelwood model, which confirmed that the degradation of BPA during the AOP followed a pseudo-first-order kinetic model (Fig. 3B). The rate constants were determined to be 0.043 and 0.119 min^{-1} in the presence of Pd NPs and Br- individually, while a substantially higher rate constant of 0.358 min^{-1} was observed when Pd NPs and Br- coexisted. Thus, the simultaneous presence of Pd NPs and Br^- synergistically contributed to the efficient removal of BPA during the AOP.

In the context of the AOP for TBBPA degradation, ROS are widely recognized as the primary species responsible for the degradation process [8,25]. When considering the individual role of Pd NPs, the introduction of MeOH (scavenger of·OH and $SO_4^{\cdot-}$) [25] resulted in a reduction in the degradation efficiency of BPA (32.8% compared to 69.2% in the control) (Fig. 3C). This observation confirms that Pd NPs can activate PMS to generate·OH and $SO_4^{\cdot-}$ for the BPA removal. However, in the presence of Br^-, the addition of MeOH did not affect the degradation efficiency of BPA, which remained at approximately 100% within 30 min. This finding suggests that·OH and $SO_4^{\cdot-}$ are not the primary reactive species in the presence of Br^-. Further analysis revealed that the addition of ammonium (scavenger of $HOBr/OBr^-$) significantly inhibited BPA degradation (21.1% compared to 100% in the control) when Br- was present individually. This inhibition effect was more pronounced than that observed in the reactors with MeOH addition or sole presence of Pd NPs, indicating that the reactive species $HOBr/OBr^-$ played a crucial role in the presence of Br^- during the AOP. Previous studies have indicated that PMS can oxidize Br- to form $HOBr/OBr^-$ with secondary rate constants of 0.7 and 0.17 $M^{-1}s^{-1}$ (Eqs. 2–3) [26], which exhibit considerable reactivity towards phenolic structures [15]. Given that BPA is a typical phenolic contaminant, the formation of $HOBr/OBr^-$ resulting from *in-situ* generated Br^- *via* the heterogeneous catalytic HDH of TBBPA over Pd NPs might be the crucial reactive species responsible for BPA degradation. Similar observations have been reported in other studies, where PMS was shown to autocatalytically convert Br^- to $HOBr/OBr^-$, effectively contributing to the removal of tetrabromobisphenol S, a compound with a structure similar to TBBPA [27].

$$HSO_5^- + Br^- \rightarrow HOBr + SO_4^{2-} \quad k = 0.7 \ M^{-1}s^{-1} \tag{2}$$

$$SO_5^{2-} + Br^- \rightarrow HOBr + SO_4^{2-} \quad k = 0.17 \ M^{-1}s^{-1} \tag{3}$$

Remarkably, the presence of the reactive species $^1O_2$ was found to significantly inhibit the degradation of BPA. As depicted in Fig. 3C, the addition of L-histidine (scavenger of $^1O_2$) [28] resulted in a decrease in BPA degradation efficiency by 92.0% and 86.4% in the presence of

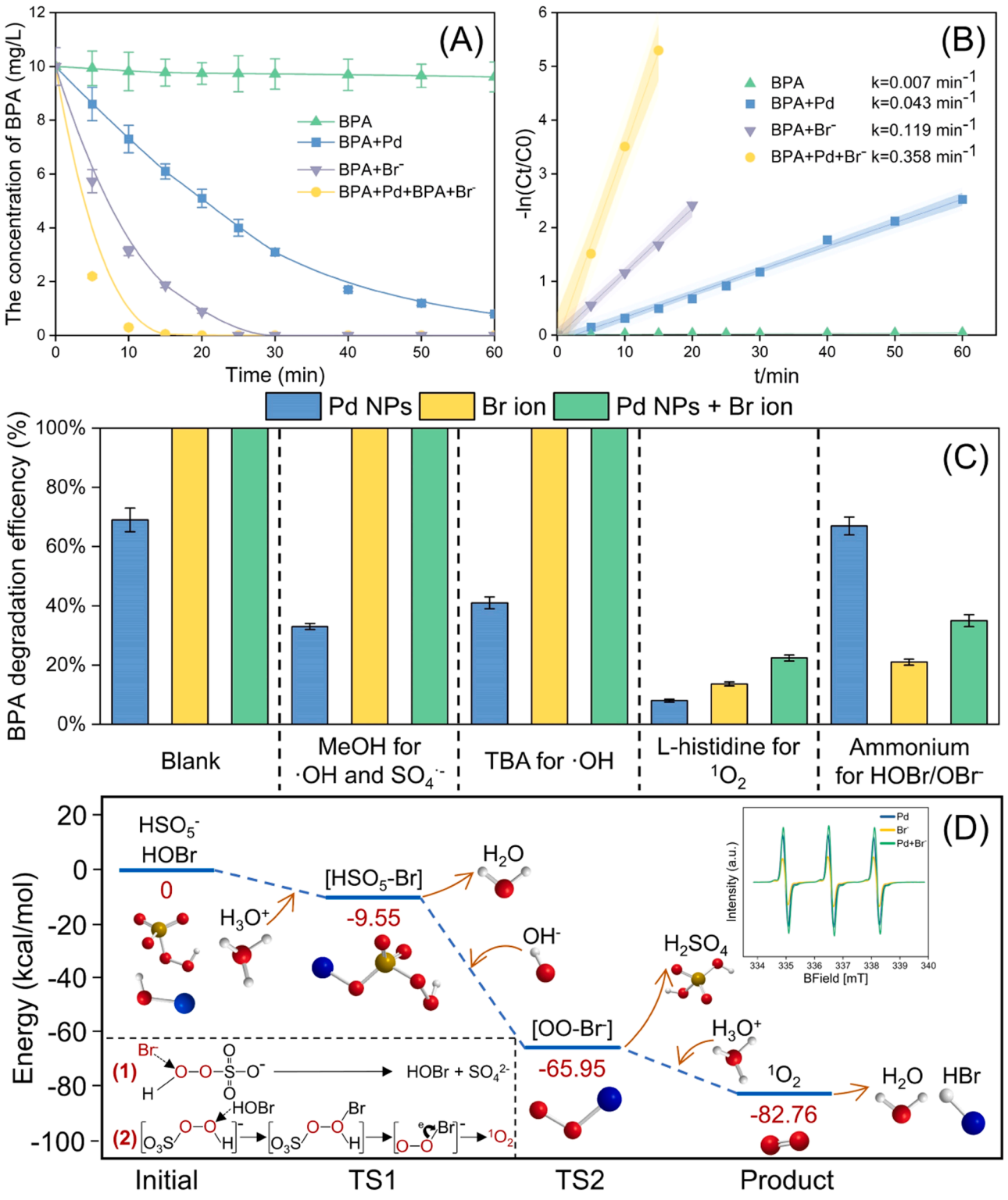

Fig. 3. The BPA degradation efficiency during the AOP in the presence of Pd NPs, Br^-, and Pd NPs+Br^- (A), the fitting curve applied by the Langmuir-Hinshelwood model (B), the effects of quenching agents on the BPA degradation in the presence of Pd NPs, Br^-, and Pd NPs+Br^- (C) (pH 5, initial BPA 10 mg/L, Pd-loading 20 mg-Pd/m^2, PMS 1 mM), and proposed mechanisms of $^1O_2$ formation from the interaction of Br^- and PMS in aqueous solution (D).

individual Pd NPs and Br^-, respectively. While the formation of $^1O_2$ through Pd NPs activation of PMS has been previously reported [11,29], the generation of $^1O_2$ by the reaction of Br^- and PMS has rarely been documented. Further EPR analysis of PMS and Br^- interaction revealed three characteristic signals with an intensity ratio of 1:1:1 (Fig. 3D), confirming the clear generation of $^1O_2$ [30]. Inspired by the previous finding, which indicated that the interaction between HOCl and PMS could induce the formation of $^1O_2$ [31], this work speculated that HOBr (structurally similar to HOCl) might also react with PMS to generate $^1O_2$. Fig. 3D illustrated the proposed mechanisms of $^1O_2$ formation *via* the interaction of Br^- and PMS. In Step 1, the nucleophilic attack of Br^- on the O atom of peroxide bond linking to H in HSO_5^- is postulated to produce

SO_4^{2-} and HOBr [15]. Then, in Step 2, the nonpolar HOBr electrophilically attacks the electronegative O atom of HSO_5^- to form [HSO_5-Br], which further converts into $OOBr^-$. Finally, $OOBr^-$ decomposes to generate $^1O_2$.

Mechanistic insights into the thermodynamic reaction of HSO_5^- and HOBr in Step 2 were obtained through DFT calculation. The corresponding free energies of intermediates and the free energy of transition states (TSs) were provided in Fig. 3D. The Br atom in HOBr, acting as the electron-deficient moiety, undergoes attachment to the O atom of peroxide bond linked to H in HSO_5^-, resulting in the formation of [HSO_5-Br] (TS1) with a spontaneous reaction energy of − 9.55 kcal/mol. Subsequently, TS1 reacts with OH^- to form $OOBr^-$ (TS2) in an exothermic process with a reaction energy of 56.40 kcal/mol. Due to its inherent instability, $OOBr^-$ rapidly dissociates into $^1O_2$ upon formation [32]. Consequently, TS2 spontaneously decomposes into $^1O_2$ with a reaction energy of − 16.82 kcal/mol. Overall, the formation of 1O2 through the reaction of HSO_5^- and HOBr is highly exothermic, with a reaction energy of 82.76 kcal/mol, confirming that it follows a thermodynamically favorable pathway. Overall, the mechanism of the BPA degradation during the AOP by Br^- and Pd NPs could be possibly divided into three pathways (Fig. 4): (1) Br^- reacted with PMS to form HOBr/OBr^-, (2) HOBr reacted with PMS to produce $^1O_2$, and (3) Pd NPs activated PMS to generate·OH, $SO_4^{\cdot-}$, and $^1O_2$. This provides an explanation for the synergistic contribution of Br^- and Pd NPs to BPA degradation during the AOP, as the rate constant in the co-presence of Pd NPs and Br^- is higher than the sum of their sole presence **(**Fig. 3**B)**.

3.4. Efficiency and degradation products of integrated HDH-AOP for TBBPA removal over Pd NPs

The efficient debromination of TBBPA through heterogeneous catalytic HDH using Pd NPs supported on a non-porous membrane, coupled with the promotion of BPA degradation during the AOP by Br^-, prompted the investigation of their combined removal efficiencies for TBBPA. Remarkably, the integrated HDH-AOP over Pd NPs demonstrated significant removal efficiency, particularly at an initial pH of 7, where nearly 99.9% of TBBPA was degraded within 30 min through catalytic HDH, followed by 99.4% BPA degradation within 15 min through the AOP (Fig. 5A). These results establish the viability of this integrated strategy for the removal of BFRs from aquatic environments. Furthermore, even after 5 cycles, the integrated HDH-AOP over Pd NPs continued to efficiently degrade 25 mg/L TBBPA within 2 h. Although the XRD or XPS intensity of Pd NPs on the non-porous membrane was slightly weaker compared to fresh Pd (Fig. 5B and C), and some miscellaneous peaks were observed (red circles in the XRD pattern), the predominant component of Pd remained as Pd(0), indicating the stable and efficient catalytic activity over prolonged reaction periods. Furthermore, the concentration of Pd in the effluent was found to be negligible, and the concentration of Pd on the surface of the membrane after the experiment was essentially equal to the initial Pd concentration. These results clearly demonstrated the considerable stability of the Pd-membrane during long-term operation.

Furthermore, the identification of intermediates generated during the integrated HDH-AOP over Pd NPs was achieved using UPLC-Q-TOF-MS. Specific information about these intermediates can be found in Table S1, while Fig. S1 provides additional details. Based on the observed intermediates, potential degradation pathways were proposed and depicted in Fig. 6A. The initial step involved the debromination of TBBPA and its conversion into BPA through catalytic HDH, which was consistent with mass balance analysis conducted in this study and previous publications [13,21,22]. Subsequently, BPA was susceptible to attack by radicals through three possible pathways. In pathway I, BPA underwent hydroxylation in the presence of·OH, leading to the formation of P1, which further transformed into P2. This hydroxylation process mediated by·OH has been reported in previous studies [33,34]. Notably, DFT calculation of the Fukui index on the nucleophilic attack (f+) of C5/C12 indicated the highest reactivity (0.0714) towards·OH attack on BPA (Fig. 6B and Table S3), further supporting the favorable formation of P1 through·OH attack. Regarding pathway II, BPA underwent β-scission, with the central carbon being attacked to generate the phenolic radical R1 and the 4-(2-hydroxyisopropyl) cationic species R2 [35]. The Fukui index on the electrophilic attack (f-) of C7/C14 was found to be exceptionally high (0.0569), indicating the vulnerability of this carbon site to electrophilic attacks from species (*e.g.*, HOBr/OBr^- and $^1O_2$) [36]. Consequently, R1 and R2 could be further oxidized into P3 and P4, respectively, by HOBr/OBr^- as described in previous literature [15]. Subsequent reactions involved the debromination of P3 into P5 and the carboxylation of P4, resulting in the formation of P6 [15,37]. Additionally, BPA could undergo ring-opening and hydroxylation processes to generate P7 [37,38] and further oxidation reactions led to the production of P8 and P9, which have been reported in the literature [39]. Finally, these individual aromatic products could undergo further ring-opening and transformation into smaller molecules, ultimately leading to the efficient removal and mineralization of TBBPA (approximately 61.2% of TBBPA was ultimately mineralized).

Furthermore, the toxicity of TBBPA and its degradation products was

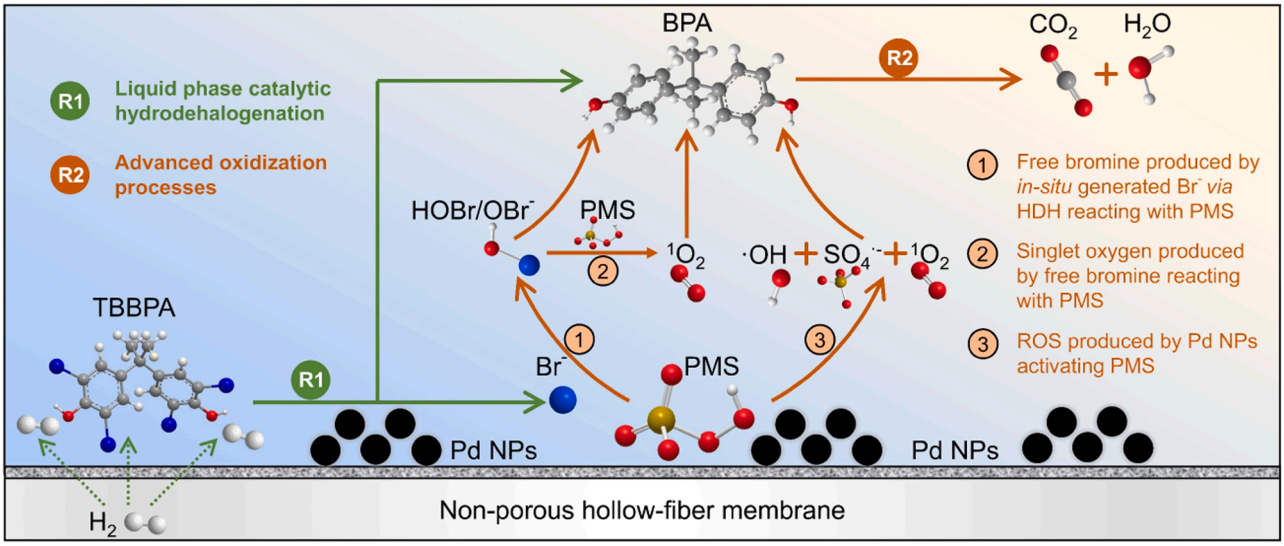

Fig. 4. The proposed degradation mechanisms of TBBPA during the integrated HDH-AOP over Pd NPs supported on the non-porous hollow-fiber membrane.

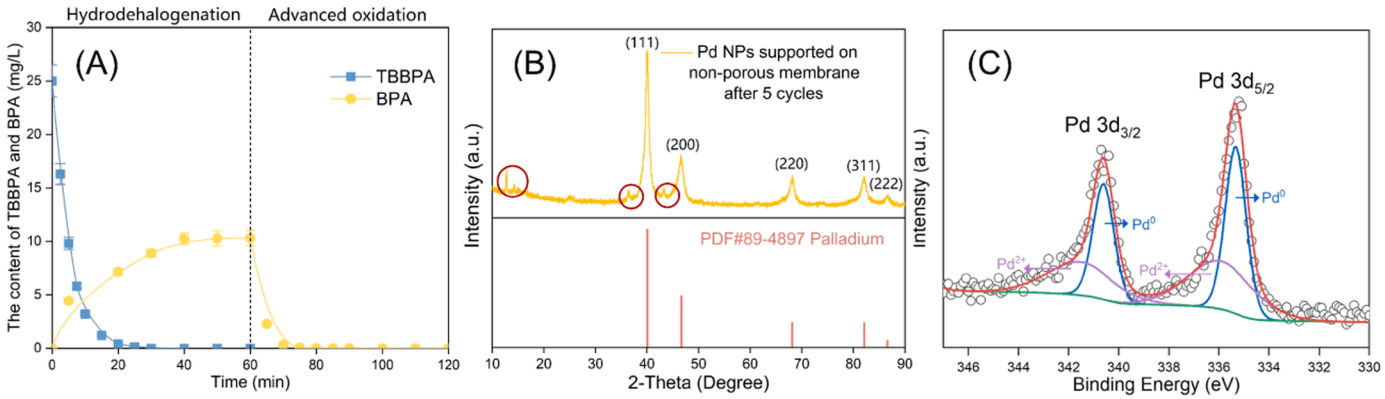

Fig. 5. The integrated HDC-AOP over Pd NPs for TBBPA degradation (pH 7, initial TBBPA 25 mg/L, Pd-loading 20 mg-Pd/m^2, gas pressure 10 psig, PMS 1 mM) (A), and the analysis of XRD (B) and XPS (C) of Pd NPs on the membrane after 5 cycles.

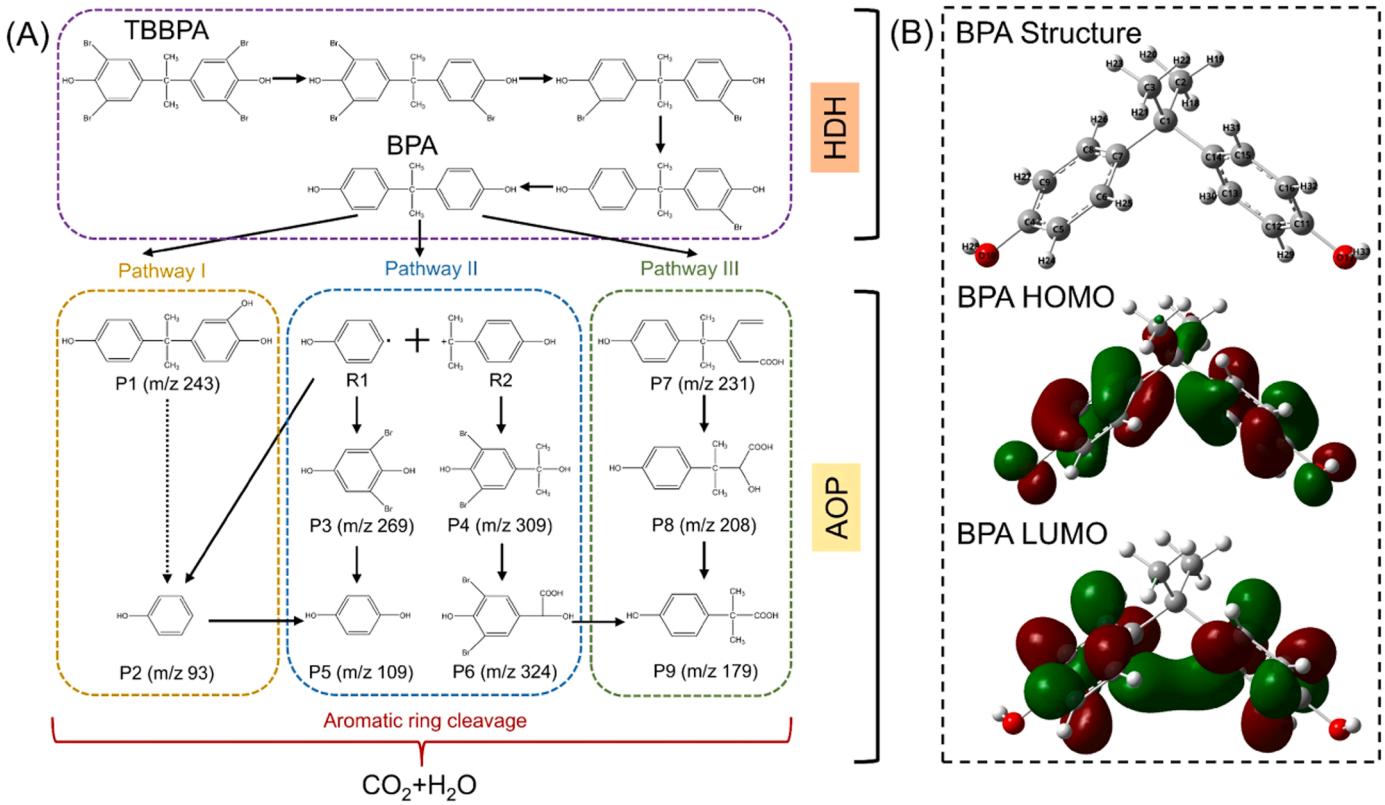

Fig. 6. The proposed TBBPA degradation pathways during the integrated HDH-AOP over Pd NPs (A), and the chemical structure, the highest occupied molecular orbitals (HOMO), and the lowest unoccupied molecular orbitals (LUMO) of BPA with the iso value of 0.04 (B).

assessed using ECOSAR, a widely used tool for predicting chemical toxicity during water treatment [40]. The results, as presented in Table S3, indicated that TBBPA exhibited the highest toxicity level, classified as "very harmful," exerting significant acute and chronic impacts. However, after the debromination of TBBPA through heterogeneous catalytic HDH over Pd NPs, the toxicity of the resulting BPA was reduced. Moreover, the AOP process further mitigated the toxicity of subsequent products, with toxicity ranging from “harmful” to “not harmful”. For instance, the carboxylation product P6 was deemed environmentally safe, showing negligible acute and chronic effects on fish, daphnids, and algae according to ECOSAR predictions (Table S3). Notably, this work observed less toxic brominated degradation products compared to previous studies related to TBBPA degradation by AOP [9, 41], possibly attributed to the advantage of complete debromination achieved through heterogeneous catalytic HDH over Pd NPs. In conclusion, the integrated HDH-AOP over Pd NPs proved to be an effective and safe method for the degradation of TBBPA, reducing its environmental risk and providing an efficient approach for the elimination of BFRs.

3.5. *Sustainability footprint and environmental implication*

The feasibility of a treatment technology depends not only on its effectiveness but also on its cost and environmental impact [42]. Therefore, the sustainability footprint of the integrated HDH-AOP over Pd NPs supported on the non-porous membrane was evaluated and compared to conventional treatment methods, including conventional HDH, AOP, adsorption, and ultrafiltration. Six discriminant criteria

were employed to assess the three pillars of sustainability: removal efficiency (R), operating cost (O), capital investment cost (C), energy consumption (E), public acceptability (P), and environmental friendliness (F). The performance of each treatment technology in these indicators was ranked on a scale from 1 to 5 (calculated based on Table S5) [16], and the overall sustainability footprint was determined by summing up the individual components using the formula $100\% \times \sum_{j=1}^{6} \left(\frac{i}{5}\right)_j \times \frac{1}{6}$ [43]. As shown in Fig. 7, despite the integrated HDH-AOP over Pd NPs supported on the membrane scoring lowest in capital investment cost, primarily due to the cost of Na_2PdCl_4, it exhibited the highest sustainability footprint (83.3%). This finding highlights the superiority and significant potential of this approach over other treatment methods, such as conventional HDH (53.3%) and ultrafiltration (66.7%), for the removal of BFRs. Further improvements in the cost of the catalyst could enhance the sustainability footprint of this method, making it even more suitable for practical applications.

Therefore, future research should focus on developing low-cost and efficient catalysts for integrated HDH-AOP on non-porous hollow-fiber membranes. One avenue to explore is the use of bimetallic catalysts with transition metals, which can enhance catalyst stability and reduce costs [44]. Additionally, single-atom catalysis could be considered, as it maximizes the utilization of metal atoms and reduces catalyst expenses [45]. Moreover, this work also demonstrated the generation of $^1O_2$ through the interaction between Br^- and PMS, presenting a novel approach for the degradation of diverse organic contaminants (*e.g.*, pharmaceuticals and pesticides) and the disinfection of viruses [46,47]. Nonetheless, caution is necessary when considering its application in treating natural water sources, as the strong oxidative property of $^1O_2$ may lead to oxidative stress and potential harm to living organisms within the aquatic ecosystem [48]. Therefore, the evaluation of the potential ecological impacts derived from $^1O_2$ is essential to ensure the responsible and sustainable use of the Br^-/PMS-induced singlet oxygen generation approach.

4. Conclusion

This work reported a novel integrated HDH-AOP approach for degrading TBBPA over Pd NPs. The heterogeneous catalytic HDH over Pd NPs could efficiently convert TBBPA into BPA and Br^- at the near-neutral condition, and the *in-situ* generated Br^- synergistically promotes BPA removal during the AOP over Pd NPs. The quenching test of free radicals indicates that free bromine ($HOBr/OBr^-$) and $^1O_2$ produced by *in-situ* generated Br^- reacting with PMS are the most important contributors to BPA degradation. Theoretical calculation confirms that the formation of $^1O_2$ through the reaction between PMS and Br^- is highly thermodynamically favorable and exergonic. Furthermore, Pd NPs exhibit considerable stability during long-term operation, and the treatment process achieved high efficiency in TBBPA mineralization with environmentally safe degradation product. Comparative analysis

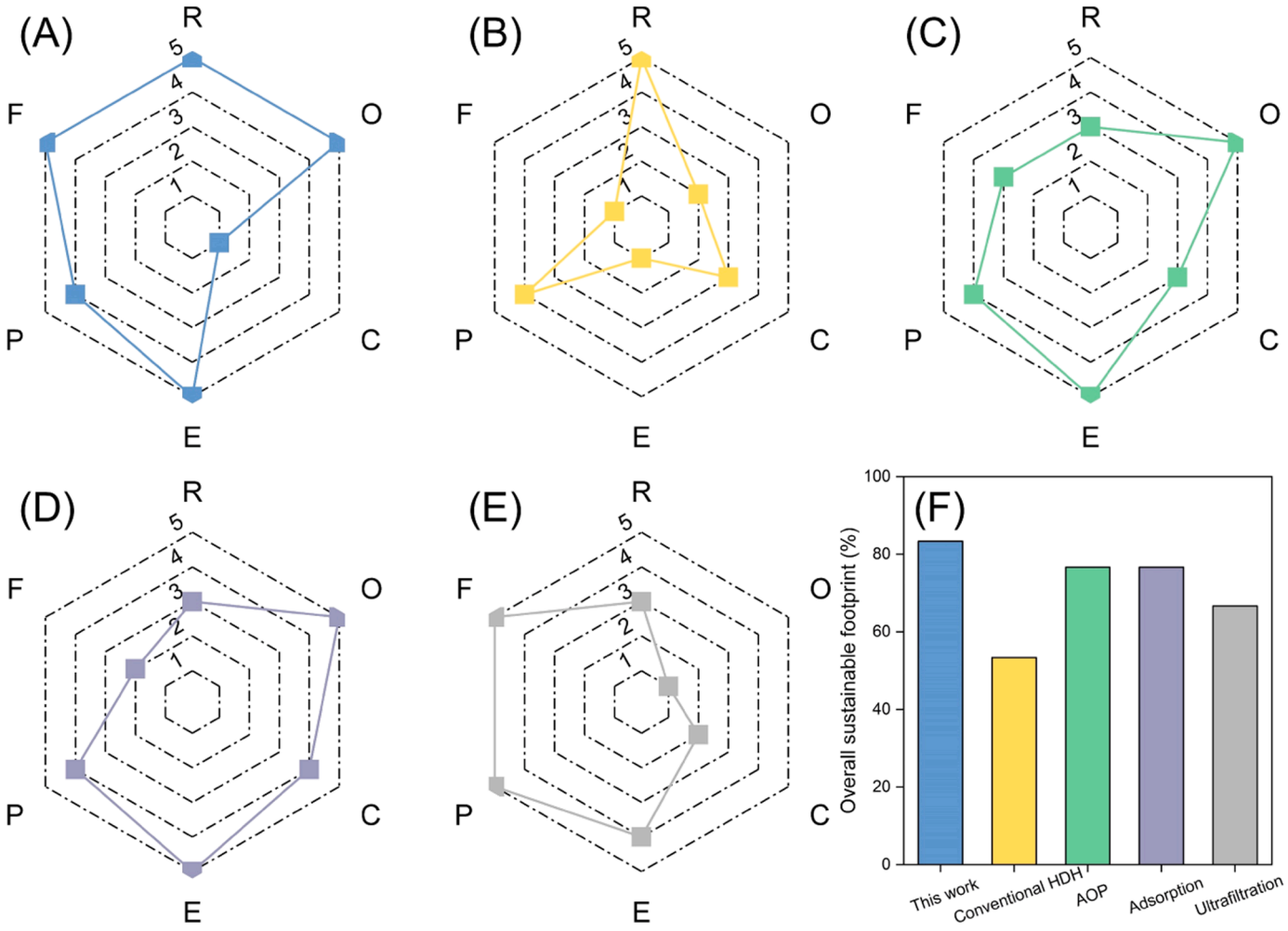

Fig. 7. The general assessment of individual treatment technologies according to the rank product statistics. This work (A), Conventional HDH (B), AOP (C), Adsorption (D), Ultrafiltration (E), and the overall sustainable footprint (F) (The characteristics considered are removal efficiency (R), operating costs (O), capital investment cost (C), energy consumed (E), public acceptability (P), and environmental friendliness (F)).

demonstrated that this novel treatment method exhibits the high sustainable footprint, as determined by the REP analysis.

CRediT authorship contribution statement

Yang Wu: Conceptualization, Data curation, Formal analysis, Funding acquisition, Investigation, Writing – original draft. **Lang Chen and Pengliang Sun**: Investigation, Methodology, Visualization. **Qingran Zhang**: Investigation, Visualization. **Yinguang Chen:** Writing – review & editing, Methodology. **Xiong Zheng**: Conceptualization, Data curation, Formal analysis, Writing – original draft.

Declaration of Competing Interest

The authors declare that they have no known competing financial interests or personal relationships that could have appeared to influence the work reported in this paper.

Data Availability

Data will be made available on request.

Acknowledgment

This work was financially supported by the National Natural Science Foundation of China (52200171), Shanghai Natural Science Foundation (22ZR1466900), and Fundamental Research Funds for the Central Universities (22120230177). The authors would like to thank Li Fan from Shiyanjia Lab (www.shiyanjia.com) for the DFT analysis.

Appendix A. Supporting information

Supplementary data associated with this article can be found in the online version at doi:10.1016/j.apcatb.2023.123213.

References

[1] J. Feiteiro, M. Mariana, E. Cairrão, Health toxicity effects of brominated flame retardants: from environmental to human exposure, Environ. Pollut. 285 (2021), 117475.
[2] H. Zhou, N. Yin, F. Faiola, Tetrabromobisphenol A (TBBPA): a controversial environmental pollutant, J. Environ. Sci. 97 (2020) 54–66.
[3] H. Feng, Y. Cheng, Y. Ruan, M.M.P. Tsui, Q. Wang, J. Jin, R. Wu, H. Zhang, P.K. S. Lam, Occurrence and spatial distribution of legacy and novel brominated flame retardants in seawater and sediment of the South China sea, Environ. Pollut. 271 (2021), 116324.
[4] J. Wang, L. Liu, J. Wang, B. Pan, X. Fu, G. Zhang, L. Zhang, K. Lin, Distribution of metals and brominated flame retardants (BFRs) in sediments, soils and plants from an informal e-waste dismantling site, South China, Environ. Sci. Pollut. Res. 22 (2) (2015) 1020–1033.
[5] H. Wu, J. Wang, Y. Xiang, L. Li, H. Qie, M. Ren, A. Lin, F. Qi, Effects of tetrabromobisphenol A (TBBPA) on the reproductive health of male rodents: A systematic review and meta-analysis, Sci. Total Environ. 781 (2021), 146745.
[6] Q. Han, W. Dong, H. Wang, H. Ma, P. Liu, Y. Gu, H. Fan, X. Song, Degradation of tetrabromobisphenol a by ozonation: Performance, products, mechanism and toxicity, Chemosphere 235 (2019) 701–712.
[7] Z. Shi, L. Zhang, Y. Zhao, Z. Sun, X. Zhou, J. Li, Y. Wu, A national survey of tetrabromobisphenol-A, hexabromocyclododecane and decabrominated diphenyl ether in human milk from China: Occurrence and exposure assessment, Sci. Total Environ. 599–600 (2017) 237–245.
[8] C. Zeng, Y. Wang, T. Xiao, Z. Yan, J. Wan, Q. Xie, Targeted degradation of TBBPA using novel molecularly imprinted polymer encapsulated C-Fe-Nx nanocomposite driven from MOFs, J. Hazard. Mater. 424 (2022), 127499.
[9] L. Wang, K. Jing, B. Hu, J. Lu, Hydrogen peroxide suppresses the formation of brominated oxidation by-products in heat-activated peroxydisulfate oxidation process, Chem. Eng. J. 417 (2021), 129138.
[10] M. Muzzio, H. Lin, K. Wei, X. Guo, C. Yu, T. Yom, Z. Xi, Z. Yin, S. Sun, Efficient hydrogen generation from ammonia borane and tandem hydrogenation or hydrodehalogenation over AuPd nanoparticles, ACS Sustain. Chem. Eng. 8 (7) (2020) 2814–2821.
[11] X. Zhou, H. Luo, Q. Chen, X. Cao, C. Shen, J. Zhou, Catalytic hydrodechlorination and advanced oxidation processes of 2,4-dichlorophenoxyacetic acid over CMK-3 supported catalyst: The bi-functional effect of metal Pd, Chem. Eng. J. 402 (2020), 126175.
[12] Y.-Y. Ahn, H. Bae, H.-I. Kim, S.-H. Kim, J.-H. Kim, S.-G. Lee, J. Lee, Surface-loaded metal nanoparticles for peroxymonosulfate activation: Efficiency and mechanism reconnaissance, Appl. Catal. B: Environ. 241 (2019) 561–569.
[13] Q. Huang, W. Liu, P.A. Peng, W. Huang, Reductive debromination of tetrabromobisphenol A by Pd/Fe bimetallic catalysts, Chemosphere 92 (10) (2013) 1321–1327.
[14] J. Luo, W. Cao, W. Guo, S. Fang, W. Huang, F. Wang, X. Cheng, W. Du, J. Cao, Q. Feng, et al., Antagonistic effects of surfactants and CeO2 nanoparticles co-occurrence on the sludge fermentation process: Novel insights of interaction mechanisms and microbial networks, J. Hazard. Mater. 438 (2022), 129556.
[15] Y. Wu, Y. Wang, T. Pan, X. Yang, Oxidation of tetrabromobisphenol A (TBBPA) by peroxymonosulfate: The role of in-situ formed HOBr, Water Res. 169 (2020), 115202.
[16] S. Bolisetty, M. Peydayesh, R. Mezzenga, Sustainable technologies for water purification from heavy metals: review and analysis, Chem. Soc. Rev. 48 (2) (2019) 463–487.
[17] W. Zhang, Y. Wu, J. Wu, X. Zheng, Y. Chen, Enhanced removal of sulfur-containing organic pollutants from actual wastewater by biofilm reactor: Insights of sulfur transformation and bacterial metabolic traits, Environ. Pollut. 313 (2022), 120187.
[18] R. Qu, M. Feng, X. Wang, Q. Huang, J. Lu, L. Wang, Z. Wang, Rapid removal of tetrabromobisphenol a by ozonation in water: Oxidation products, reaction rathways and toxicity Assessment, PLOS ONE 10 (10) (2015), e0139580.
[19] Y. Luo, C. Zhou, Y. Bi, X. Long, B. Wang, Y. Tang, R. Krajmalnik-Brown, B. E. Rittmann, Long-term continuous co-reduction of 1,1,1-trichloroethane and trichloroethene over palladium nanoparticles spontaneously deposited on H_2-transfer membranes, Environ. Sci. Technol. 55 (3) (2021) 2057–2066.
[20] F. Zhang, S. Miao, Y. Yang, X. Zhang, J. Chen, N. Guan, Size-dependent hydrogenation selectivity of nitrate on Pd-Cu/TiO_2 catalysts, J. Phys. Chem. C. 112 (20) (2008) 7665–7671.
[21] K. Wu, M. Zheng, Y. Han, Z. Xu, S. Zheng, Liquid phase catalytic hydrodebromination of tetrabromobisphenol A on supported Pd catalysts, Appl. Surf. Sci. 376 (2016) 113–120.
[22] X.-Q. Lin, Z.-L. Li, Y.-Y. Zhu, F. Chen, B. Liang, J. Nan, A.-J. Wang, Palladium/iron nanoparticles stimulate tetrabromobisphenol a microbial reductive debromination and further mineralization in sediment, Environ. Int. 135 (2020), 105353.
[23] Z. Huang, D. Deng, J. Qiao, Y. Ju, Y. Chen, D.D. Dionysiou, New insight into the cosolvent effect on the degradation of tetrabromobisphenol A (TBBPA) over millimeter-scale palladised sponge iron (Pd-s-Fe0) particles, Chem. Eng. J. 361 (2019) 1423–1436.
[24] Z. Zhang, Y. Liu, Y. Zhang, R. Li, Y. Guan, Activation persulfate for efficient tetrabromobisphenol A degradation via carbon-based materials: Synergistic mechanism of doped N and Fe, J. Hazard. Mater. 455 (2023), 131471.
[25] H. Chi, J. Wan, X. Zhou, J. Sun, B. Yan, Fe@C activated peroxymonosulfate system for effectively degrading emerging contaminants: Analysis of the formation and activation mechanism of Fe coordinately unsaturated metal sites, J. Hazard. Mater. 419 (2021), 126535.
[26] G. Lente, J. Kalmár, Z. Baranyai, A. Kun, I. Kék, D. Bajusz, M. Takács, L. Veres, I. Fábián, One- Versus two-electron oxidation with peroxomonosulfate ion: Reactions with iron(II), vanadium(IV), halide ions, and photoreaction with cerium (III), Inorg. Chem. 48 (4) (2009) 1763–1773.
[27] H. Xu, L. Meng, X. Zhao, J. Chen, J. Lu, J.-M. Chovelon, Y. Ji, Accelerated oxidation of the emerging brominated flame retardant tetrabromobisphenol S by unactivated peroxymonosulfate: The role of bromine catalysis and formation of disinfection byproducts, Water Res. 204 (2021), 117584.
[28] L. Gao, Y. Guo, J. Zhan, G. Yu, Y. Wang, Assessment of the validity of the quenching method for evaluating the role of reactive species in pollutant abatement during the persulfate-based process, Water Res. 221 (2022), 118730.
[29] Y. Wang, D. Cao, M. Liu, X. Zhao, Insights into heterogeneous catalytic activation of peroxymonosulfate by Pd/g-C_3N_4: The role of superoxide radical and singlet oxygen, Catal. Commun. 102 (2017) 85–88.
[30] A. Wang, B.-Z. Zhu, C.-H. Huang, W.-X. Zhang, M. Wang, X. Li, L. Ling, J. Ma, J. Fang, Generation mechanism of singlet oxygen from the interaction of peroxymonosulfate and chloride in aqueous systems, Water Res. 235 (2023), 119904.
[31] S. Wang, J. Wang, Treatment of membrane filtration concentrate of coking wastewater using PMS/chloridion oxidation process, Chem. Eng. J. 379 (2020), 122361.
[32] J.S. Francisco, J.N. Crowley, Theoretical Investigation of product channels in the CH_3O_2 + Br reaction, J. Phys. Chem. A 110 (10) (2006) 3778–3784.
[33] M. Cao, P. Wang, Y. Ao, C. Wang, J. Hou, J. Qian, Photocatalytic degradation of tetrabromobisphenol A by a magnetically separable graphene-TiO_2 composite photocatalyst: Mechanism and intermediates analysis, Chem. Eng. J. 264 (2015) 113–124.
[34] C. Guan, J. Jiang, S. Pang, X. Chen, R.D. Webster, T.-T. Lim, Facile synthesis of pure g-C_3N_4 materials for peroxymonosulfate activation to degrade bisphenol A: Effects of precursors and annealing ambience on catalytic oxidation, Chem. Eng. J. 387 (2020), 123726.
[35] Y.-M. Kang, M.-K. Kim, K.-D. Zoh, Effect of nitrate, carbonate/bicarbonate, humic acid, and H_2O_2 on the kinetics and degradation mechanism of Bisphenol-A during UV photolysis, Chemosphere 204 (2018) 148–155.
[36] Y. Li, J. Qi, J. Shen, B. Wang, J. Kang, P. Yan, Y. Cheng, L. Li, L. Shen, Z. Chen, Non-radical dominated degradation of bisphenol S by peroxymonosulfate activation under high salinity condition: Overlooked HOCl, formation of intermediates, and toxicity assessment, J. Hazard. Mater. 435 (2022), 128968.
[37] Y. Zhang, Z. Chen, L. Zhou, P. Wu, Y. Zhao, Y. Lai, F. Wang, S. Li, Efficient electrochemical degradation of tetrabromobisphenol A using MnO2/MWCNT

composites modified Ni foam as cathode: Kinetic analysis, mechanism and degradation pathway, J. Hazard. Mater. 369 (2019) 770–779.
[38] Y. Wang, Y. Wu, Y. Yu, T. Pan, D. Li, D. Lambropoulou, X. Yang, Natural polyphenols enhanced the Cu(II)/peroxymonosulfate (PMS) oxidation: The contribution of Cu(III) and HO•, Water Res. 186 (2020), 116326.
[39] W.H.M. Abdelraheem, X. He, Z.R. Komy, N.M. Ismail, D.D. Dionysiou, Revealing the mechanism, pathways and kinetics of UV254nm/H_2O_2-based degradation of model active sunscreen ingredient PBSA, Chem. Eng. J. 288 (2016) 824–833.
[40] S. Shao, L. Qian, X. Zhan, M. Wang, K. Lu, J. Peng, D. Miao, S. Gao, Transformation and toxicity evolution of amlodipine mediated by cobalt ferrite activated peroxymonosulfate: Effect of oxidant concentration, Chem. Eng. J. 382 (2020), 123005.
[41] L. Wang, D. Kong, Y. Ji, J. Lu, X. Yin, Q. Zhou, Formation of halogenated disinfection byproducts during the degradation of chlorophenols by peroxymonosulfate oxidation in the presence of bromide, Chem. Eng. J. 343 (2018) 235–243.
[42] C.A. Robbins, X. Du, T.H. Bradley, J.C. Quinn, T.M. Bandhauer, S.A. Conrad, K. H. Carlson, T. Tong, Beyond treatment technology: Understanding motivations and barriers for wastewater treatment and reuse in unconventional energy production, Resour., Conserv. Recycl. 177 (2022), 106011.
[43] A. Palika, A. Armanious, A. Rahimi, C. Medaglia, M. Gasbarri, S. Handschin, A. Rossi, M.O. Pohl, I. Busnadiego, C. Gübeli, et al., An antiviral trap made of protein nanofibrils and iron oxyhydroxide nanoparticles, Nat. Nanotechnol. 16 (8) (2021) 918–925.
[44] J. Nieto-Sandoval, M. Munoz, Z.M. de Pedro, J.A. Casas, Application of catalytic hydrodehalogenation in drinking water treatment for organohalogenated micropollutants removal: A review, J. Hazard. Mater. Adv. 5 (2022), 100047.
[45] B. Huang, Z. Wu, H. Zhou, J. Li, C. Zhou, Z. Xiong, Z. Pan, G. Yao, B. Lai, Recent advances in single-atom catalysts for advanced oxidation processes in water purification, J. Hazard. Mater. 412 (2021), 125253.
[46] Y. Bu, H. Li, W. Yu, Y. Pan, L. Li, Y. Wang, L. Pu, J. Ding, G. Gao, B. Pan, Peroxydisulfate activation and singlet oxygen generation by oxygen vacancy for degradation of contaminants, Environ. Sci. Technol. 55 (3) (2021) 2110–2120.
[47] L. Kong, G. Fang, X. Xi, Y. Wen, Y. Chen, M. Xie, F. Zhu, D. Zhou, J. Zhan, A novel peroxymonosulfate activation process by periclase for efficient singlet oxygen-mediated degradation of organic pollutants, Chem. Eng. J. 403 (2021), 126445.
[48] V. Dogra, M. Li, S. Singh, M. Li, C. Kim, Oxidative post-translational modification of EXECUTER1 is required for singlet oxygen sensing in plastids, Nat. Commun. 10 (1) (2019) 2834.